Results in Physics 17 (2020) 103132

Contents lists available at ScienceDirect

Results in Physics

journal homepage: www.elsevier.com/locate/rinp

Effect of substrate temperature on the properties of RF sputtered CdS thin films for solar cell applications

N.K. Das[a], J. Chakrabartty[a,b,*], S.F.U. Farhad[c], A.K. Sen Gupta[a], E.M.K. Ikball Ahamed[a], K.S. Rahman[d,e], A. Wafi[e], A.A. Alkahtani[e], M.A. Matin[a], N. Amin[e]

[a] Department of Electrical and Electronic Engineering, Chittagong University of Engineering and Technology, Chittagong 4349, Bangladesh
[b] Institut National de la Recherché Scientifique (INRS), 1650, Boulevard Lionel Boulet, Varennes, Quebec J3X 1S2, Canada
[c] Industrial Physics Division, Bangladesh Council of Scientific and Industrial Research (BCSIR), Dhaka 1205, Bangladesh
[d] Solar Energy Research Institute, Universiti Kebangsaan Malaysia, 43600 Bangi, Selangor, Malaysia
[e] Institute of Sustainable Energy, Universiti Tenaga Nasional (@The Energy University), Jalan IKRAM-UNITEN, 43000 Kajang, Selangor, Malaysia

ARTICLE INFO

Keywords:
Thin films
CdS
RF sputtering
Substrate temperature
XRD
UV–VIS-NIR
Hall effect measurement

ABSTRACT

We report the effect of substrate temperature (25–300 °C) on the structural, optical and electrical properties of Cadmium Sulphide (CdS) thin films deposited onto glass substrate by Radio Frequency (RF) magnetron sputtering. The structural, morphological, optical and electrical properties of the films were characterized by X-ray diffraction (XRD), Field emission scanning electron microscopy (FE-SEM), UV–VIS-NIR spectroscopy and Hall Effect measurement respectively. The XRD studies showed that the films were polycrystalline with hexagonal wurtzite structure preferentially oriented along the (0 0 2) plane parallel to the substrate surface. The XRD data analysis further revealed the crystallite size of the nanocrystalline films i.e. 22–24 nm exhibiting the fact that crystallite size increased with increasing the substrate temperature. The FE-SEM images along with energy dispersive spectroscopy (EDS) studies confirmed the homogeneous, compact and pin-hole free surface morphology. The UV–VIS-NIR studies unveiled the optical transmittance in the range of 75–90% after 540 nm of the wavelength of light. The optical band gaps were found to be decreasing from 2.34 eV to 2.26 eV with increasing the substrate temperature. The films were characterized as n-type as evidenced by the Hall Effect measurement. The carrier mobility was found to be increasing gradually from 5.53 to 12.57 $cm^2/V{\cdot}s$ by increasing the substrate temperature from room temperature to 300 °C due to the improvement of crystalline quality and grain size of the films. The results showed good optical and electrical properties of the films deposited at 300 °C which are suitable to use as window layer in thin film based solar cells.

Introduction

The primary function of a window layer of a thin-film solar cell is to form a junction with the absorber layer while admitting a maximum amount of light into the junction region and the absorber layer. In CdTe solar cells, proper material selection and optimization of window layer are important as it plays a vital role to transmit light into absorber layer. Generally, a wide band gap semiconductor with low thickness (typically in the range of 50–100 nm) is employed in the cell structure as window layer to achieve high optical throughput and minimum resistive losses [1]. CdS is a wide band gap material (~2.42 eV) and is used widely as a n-type thin window layer in CdTe thin-film solar cells [1–4]. CdS grows intrinsically as n-type due to the presence of intrinsic donor defects i.e. S vacancies and Cd interstitials in the films [5]. Due to the higher miscibility with hetero-partners [6–8], it is incorporated as a sandwich layer between the absorber and transparent conducting oxide (TCO) layer in solar cell devices. The favourable crystal symmetry, higher optical transparency, suitable band gap, higher thermal and chemical stability, and easy doping process (can reach over 10^{19} cm^{-3}) enable numerous optoelectronic properties in CdS thin films that are extremely useful in optoelectronic devices including solar cells. Moreover, incorporating thin CdS layer is crucial for the devices because thin CdS layer as compared to their thick counterpart allows to transmit more efficiently the blue region of the light spectrum into the active layer which eventually enhances the short circuit current density [9–12].

* Corresponding authors at: Department of Electrical and Electronic Engineering, Chittagong University of Engineering and Technology, Chittagong 4349, Bangladesh.
E-mail addresses: chakrabartty@emt.inrs.ca, joychakr@cuet.ac.bd (J. Chakrabartty).

https://doi.org/10.1016/j.rinp.2020.103132
Received 6 January 2020; Received in revised form 19 April 2020; Accepted 21 April 2020
Available online 30 April 2020

For the synthesis of CdS thin films, several chemical and physical methods have been employed including Chemical Bath Deposition (CBD), DC and RF Sputtering, Electrodeposition (ED), Close-Spaced Sublimation (CSS), Metal-Organic Chemical Vapour Deposition (MOCVD) [13–18] etc. Among all deposition methods, RF sputtering method is recognized as one of the most suitable methods to deposit a very thin layer of CdS in Ar or He ambient [19]. It allows to deposit large area CdS films at low substrate temperature and provides better adhesion, high uniformity, and controllable thickness on the template of interest. It also permits to synthesis films at moderate substrate temperature, scalable for the in-line production and relatively easier waste handling than other solution-based methods [19,20]. The deposition parameters of RF sputtering method that mostly influence the nucleation and growth of CdS films are RF power, substrate temperature, source to substrate distance, deposition time, and gas flow during deposition. Genişel et al. reported the effect of substrate temperature on the quality of CdS thin films describing the growth of hexagonal wurtzite crystal structure oriented along (0 0 2) plane, where the crystallinity and the surface roughness increased with increasing the substrate temperature i.e. from 40 °C to 275 °C [20]. Kim et al. reported the deposition of CdS films at different substrate temperatures (at 100 °C, 200 °C, 300 °C, 400 °C and 500 °C) illustrating the fact that the surface uniformity and optical transmittance decreased in the films which were deposited over 300 °C [21]. Rondiya et al. reported CdS films deposited at room temperature (25 °C) where the electrical resistivity and surface roughness increased with the deposition time [22], wherein similar results had been claimed by Li et al. at much higher temperature (300 °C) [23]. Nonetheless, the oxygen gas flow during deposition (Ar:O_2 ratio: 0–4%) may result in increased nanocrystallinity and band gap of the films [6–10,24]. All these reported results indicate that the physical properties and crystal qualities of the CdS films are strongly dependent on the deposition parameters. Specifically, the elevated substrate temperature is a crucial indicator to understand the crystal quality and the physical properties of the CdS films. Despite the availability of the numerous reports that described the effect of substrate temperature on the structure, optical and electrical properties, the relation between the variation of deposition parameter and the resulting film properties has not been fully elucidated yet.

In this report, we systematically present a complete study of the effect of substrate temperature on microstructure, morphology, optical and electrical properties of as-synthesized CdS thin films. The films were deposited onto glass substrates at 25 °C, 250 °C, 275 °C and 300 °C using RF sputtering method under Ar atmosphere. The crystal structure, micro strain, and dislocation density of the films were characterized by XRD analysis. The UV–Vis spectroscopy and the Hall Effect measurement set up were employed to estimate the band gap and the electron mobility of the films. The results show that the crystallite size increases with increasing substrate temperature and thus reducing the grain boundaries in the films. As a result, the resistivity of the films decreases. Our findings demonstrate that the optimization of the substrate temperature, optical and electrical properties of the films is a novel and original study that is useful either for solar cell applications or for other optoelectronic device applications.

Experimental details

The CdS thin films were deposited on the standard borosilicate glass by RF magnetron sputtering technique at different substrate temperatures with a base pressure of 5×10^{-6} Torr. Initially, the glasses were mechanically scrubbed and clean in the ultra-sonic cleaner by warm detergent water followed by the conventional solvent in a sequence of methanol, acetone, methanol and deionized water for 15 min at 50 °C temperature. After that, the cleaned glasses were dried by compressed dry nitrogen and subsequently air annealed on a hot plate at a temperature of 100 °C for 5 min to eliminate moisture. The dried glasses were mounted to a substrate holder in NSC-3500, 2 guns RF sputtering machine. The distance between the CdS target and substrate was kept fixed at 7 cm for all depositions. The CdS films were deposited in Argon ambient with process pressure of 3.54 mTorr from a 50 mm diameter CdS target. The purity of the CdS target was 99.99%. During the deposition, the thickness of the films was monitored by the Quartz Crystal Deposition Monitor (QCM). The RF power of the CdS target was set to 30 W and the thicknesses of all the as-grown films were approximately 100 nm. During the deposition, the flow of Ar gas was maintained at 16 sccm by Mass Flow Controller (MFC). The CdS deposition process parameters are presented in Table 1. After deposition, the as-grown CdS thin films were subjected to air annealing at 100 °C for 10 min. The thicknesses of the as-grown CdS thin films were checked by the Dektak stylus profilometer. The optical, structural, morphological and electrical properties of the as-grown CdS films were inspected by UV–VIS-NIR, XRD, FE-SEM, and Hall Effect measurement system respectively.

Table 1
CdS thin films deposition parameter.

Process parameters	Value
RF power	30 W
Deposition pressure	3.54 mTorr
Ar gas flow	16 sccm
Substrate temperature	25–300 °C
Thickness (approximate)	100 nm
Deposition time (approximate)	30 min
Source to substrate distance	7 cm

Results and discussion

Structural analysis

The crystal structure of the RF-sputtered CdS thin films deposited at different substrate temperatures were analyzed by advanced 'BRUKER AXS-D8 diffractometer in Bragg-Brentano geometry with Cu-k_α X-ray radiation source ($\lambda = 0.15408$ nm). The XRD patterns of the films deposited at 25 °C, 250 °C, 275 °C, and 300 °C are shown in Fig. 1. All the XRD peaks showed polycrystalline nature exhibiting predominant peaks at ~26.92° and ~47.90° respectively. The peaks were assigned to the hexagonal wurtzite crystal structure with a preferential crystal orientation along the (0 0 2) plane, which is a good agreement with the previously reported results [7,17–24]. The hexagonal wurtzite crystal structure oriented in (0 0 2) plane is more stable compared to cubic structure and is considered as an advantage for solar cell applications [5,25].

The lattice constant, grain size, micro-strain, crystal phases, and dislocation densities of the as-deposited films were calculated from the XRD spectra. The Bragg's law is used to calculate the lattice constant of the crystalline thin films. The lattice spacing of (0 0 2) oriented hexagonal wurtzite crystals and the equivalent lattice constant of a cubic crystal can be co-related from the following Eqs. (1) and (2),

$$d_{hkl} = \frac{n\lambda}{2\sin\theta} \tag{1}$$

$$a_c = d_{hkl}(h^2 + k^2 + l^2)^{1/2} \tag{2}$$

where n, d, and θ represents positive integer, inter planar spacing, and the angle between the adjacent crystal planes respectively. Afterward, the out of plane and in plane lattice constant c, and a of hexagonal unit cell can be calculated from the Vegard's law, as described by Eq. (3a) and Eq. (3b) respectively:

$$a_{hex} = \left(\frac{1}{2}\right)^{\frac{1}{2}} a_{cubic} \tag{3a}$$

and

$$c_{hex} = \left(\frac{4}{3}\right)^{\frac{1}{2}} a_{cubic} \tag{3b}$$

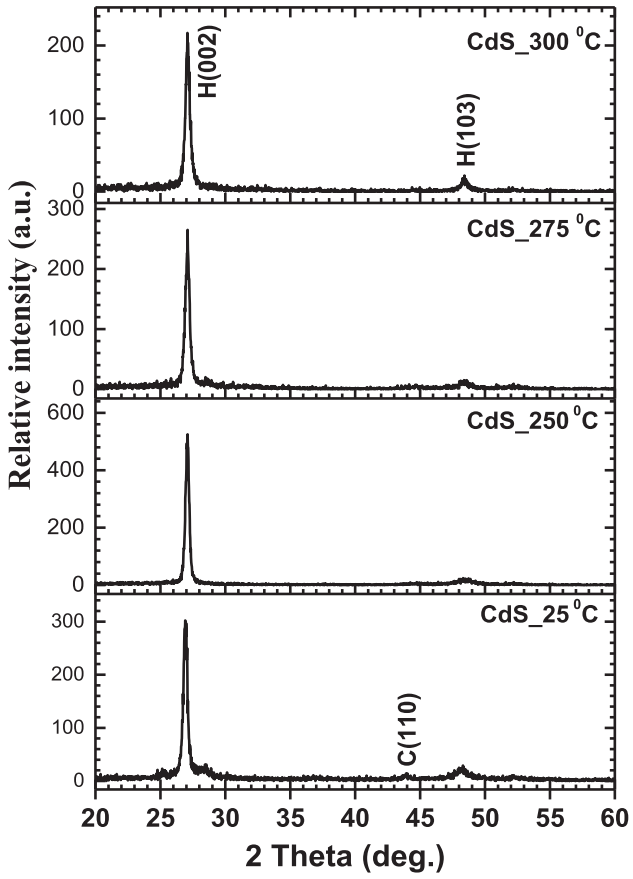

Fig. 1. XRD patterns of CdS thin films grown at different substrate temperatures.

Nonetheless, the crystallite size D of the CdS films was estimated by using Scherrer formula as shown in Eq. (4):

$$D_{hkl} = \frac{K\lambda}{\beta_{2\theta}\cos\theta} \tag{4}$$

where K is the Scherrer's constant which is subjected to the process of the width measurement, the size distribution, and the shape of the crystals. Generally, the numerical value of K for spherical crystallites is of ~0.89, and $\beta_{2\theta}$ is the width of diffraction peak in radians at a height halfway between backgrounds.

The dislocation densities of the films were computed by using Williamson and Smallman's relation [26] as shown in Eq. (5),

$$\delta = \frac{n}{D^2} \tag{5}$$

where n is a factor which is considered as unity for minimum dislocation densities.

The calculated values of the lattice constant, average crystallite size, micro-strain, and the dislocation densities are presented in Table 2.

In RF sputtering method, the atoms or ions eject from the target material due to the interaction of high energy Ar^+ ions present in the deposition chamber with the target material. These ejected atoms or ions travelled through the ambient gas environment and reached to the surface of the substrate which eventually condensed onto the substrate surface. Thereafter, the condensation, nucleation and crystallization processes of the adatoms occurred which resulted in the formation of the desired nanostructures on the substrate i.e. in our case thin films. In principle, the mobility of the adatoms among other factors dominate the condensation, nucleation and crystallization processes in RF sputtering method. The microstructure and morphology of the films be governed by the kinetics of the mobile adatoms on the substrate which can be controlled by the substrate temperature, process pressure, bias voltage applied to the substrate as well as the thermal characteristics of the target material [27].

While keeping the other deposition parameter of the films constant, the mobility as well as diffusion rate of the adatoms arrived at the surface of the substrate increase with elevating the substrate temperature. At low substrate temperature, initially the columnar microstructures are likely to be formed on the substrate surface due to the low mobility and low diffusion rate of the adatoms. As the substrate temperature increases, both the mobility and diffusion rate of the adatoms increase which leads to the formation of the grains and thus increasing the size of the grains by producing a dense microstructure with a higher degree of binding among the columnar microstructures and the borders between that columnar microstructures. When the temperature increases further, the diffusion rate onto the grains increases, leading to the recrystallization of the adatoms which influence the morphology of the films. As result, smooth surface morphology with increased crystallite size are observed in the deposited films (Table 2). These observation is in good agreement with the reported results on the growth of CdS thin films at different temperatures by RF sputtering method [21], the solvothermal method [28], CBD [29,30], and the thermal evaporator method [31].

As can be seen in Table 2, both micro-strain and dislocation densities decreases with increasing the substrate temperature. These observations have also been reported in previous publications [28–31,33]. Generally, the RF-sputtered CdS thin films possess a large number of nanocrystals. As result, a large number of randomly deposited grains with different crystal orientations appears and thus induces micro-strain in the films [11,32]. In our case, the crystal reorientation and reduction of point defects in crystal at elevated temperature might be the reason of decreasing micro-strain and dislocation densities [13].

Morphological and compositional properties

The morphological properties of all the deposited films were carried out by Field Emission Scanning Electron Microscope (FE-SEM). The FE-SEM micrographs of the as-deposited CdS thin films are presented in Fig. 2. All the films are uniformly deposited on glass substrate without micro-crack and pin holes as shown in Fig. 2. The grain size estimated by ImageJ software were found to be in the range of 46–80 nm (average ~64 ± 12 nm), 66–98 nm (average ~80 ± 10 nm), 70–105 nm (average ~84 ± 12 nm), and 97–152 nm (average ~135 ± 19 nm) for thin films grown at 25 °C, 250 °C, 275 °C, and 300 °C respectively. This observation suggests the recrystallization of CdS grains at elevated temperatures which is consistent with crystallite size increasing trend as observed in the XRD analysis.

The elemental compositions of the sputtered CdS thin films were

Table 2
Crystallite size, micro-strain and dislocation densities of the as-grown CdS films.

Substrate temperature (°C)	d_{hkl} [0 0 2] Å	a [0 0 2] Å	c [0 0 2] Å	Crystallite size D (nm)	Micro –strain $\varepsilon(\times 10^{-3})$	Dislocation density δ ($\times 10^{12}$ cm^{-2})
25	3.31	4.67	7.63	22.87	6.51	1.91
250	3.28	4.64	7.58	23.49	6.30	1.81
275	3.28	4.64	7.58	24.16	6.12	1.71
300	3.29	4.65	7.59	24.58	6.02	1.66

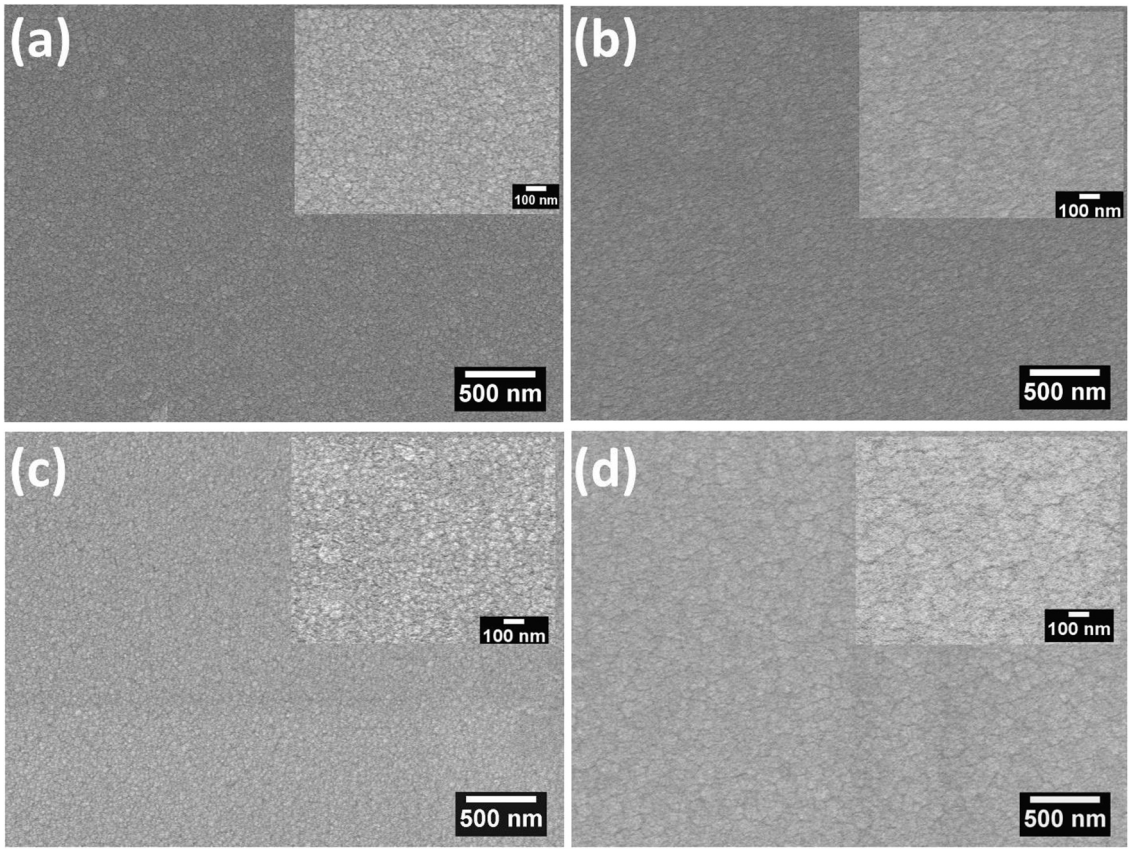

Fig. 2. SEM micrograph of CdS thin films at (a) 25 °C, (b) 250 °C, (c) 275 °C, and (d) 300 °C. The inset shows the zoomed area of the respective samples.

obtained by EDX coupled with the FE-SEM as shown in Fig. 3. For each sample, three different points on the sample surfaces were selected to record the EDX spectra. Later, the quantified data from the spectra were averaged to make the elemental composition which are attached as inset table in Fig. 3. All the CdS films were composed of slight Cd-rich stoichiometry. The atomic percentage of Cd was consistently decreasing with increasing substrate temperature and a nearly stoichiometric condition (Cd:S: 51.88: 48.12) was achieved at 300 °C. This elemental ratio is reasonably well matched with the chemical formula of CdS which are consistent with other reports as well [17,28,34,35]. The reduction of Cd content in CdS thin film with increasing substrate temperature presumably due to the escaping of Cd atom from the film surface, as the surface mobility and vapor pressure of Cd is greater than that of S_2 [36].

Optical properties

The effect of substrate temperatures on the optical properties was observed by UV–VIS-NIR spectrometer (PerkinElmer UV WinLab) in the wavelength range of 300–1200 nm. The transmission spectra are presented in Fig. 4. A sharp transition in optical transmission near the band edge of 520 nm is observed which indicates the better crystallinity for the as-grown samples. The films grown at 25 °C exhibited the highest percentage of optical transmission (70–90%) in the wavelength range of 520–840 nm along with an indication of the transmission of short wavelength of sunlight (300–400 nm). The combined transmission of short and visible wavelengths of solar spectrum is certainly beneficial for enhancing the light absorption of the cell. This optical transmission of the films grown at room temperature is found to be better than the previously reported results [22–24,37,38]. The CdS thin films deposited at higher substrate temperatures compared to the films deposited at room temperature showed superior optical transmission only in the long-wavelength region.

The absorption coefficient (α) of all the films is estimated using the following relationship,

$$\alpha = \frac{1}{t}\ln\left(\frac{1}{T}\right) \tag{6}$$

where T and t represents percentage of transmission and the film thickness, respectively. The relationship between absorption coefficient (α) and optical band gap (E_g) of the films can be expressed by the following equation [39].

$$(\alpha h\nu)^{\frac{1}{m}} = K(h\nu - E_g) \tag{7}$$

where 'K' is energy independent constant depends on the nature of transition occurring in the films, 'h' is plank constant and 'ν' is photon frequency of the illuminated radiation. In Eq. (7), m is a factor which is used to indicate the mode of transition occurring in thin films. Eq. (7) may be rewritten as;

$$\frac{d(\ln \alpha h\nu)}{d(h\nu)} = \frac{m}{h\nu - E_g} \tag{8}$$

The value of m is estimated from the slope of ln(αhν) versus ln(hν-Eg) plot as shown in Fig. 4(b). The calculated value of m for as-grown CdS thin films is 0.49, 0.44, 0.44 and 0.45 respectively for substrate temperature 25–300 °C, which indicates the allowed direct transition in the deposited CdS thin films. The optical band gap (E_g) of all the CdS thin films is calculated by plotting square of absorption coefficient times the photon energy versus incident photon energy (Fig. 5) commonly known as "Tauc" plot [39]. As shown in Fig. 5, the optical absorption approaches near to zero at lower photon energies but not absolutely zero. This phenomenon is commonly termed as "Urbach" tail effect [40–42]. Near the band gap region, the CdS films show linearity of its squared exponent plot which is an indication of strong absorption

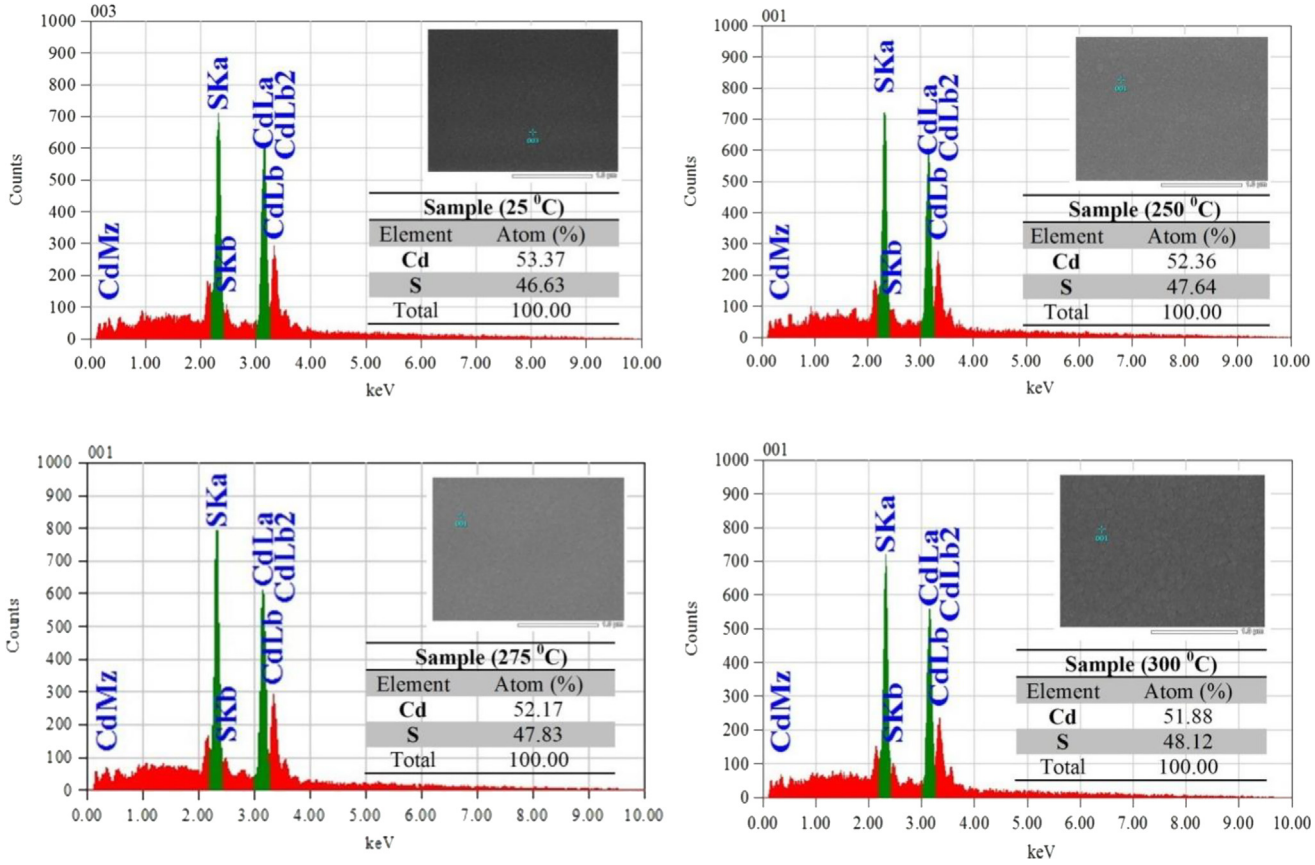

Fig. 3. Plots of EDX micro-analyses of CdS thin films deposited at 25 °C, 250 °C, 275 °C, and 300 °C. Inset shows the SEM images with same magnification (scale bar: 1 μm) and atomic percentage of Cd and S of the respective sample.

whereas the absorption saturates at higher photon energies and the curve deviates from its linearity. The E_g is estimated by extrapolating the linear portion of $(\alpha h\nu)^2$ to the X-axis. The band gap for the films deposited at 25 °C, 250 °C, 275 °C and 300 °C is estimated to 2.34 eV, 2.30 eV, 2.28 eV and 2.26 eV respectively. These optical band gaps match well with the previously reported works [37,38]. It is observed that the band gap of deposited CdS thin films decreased slightly with substrate temperature presumably due to the increment of crystallite size [43].”

Electrical properties

The electrical properties of the deposited CdS thin films were inspected by the Hall Effect measurement at room temperature under dark condition. The measured values of carrier concentration, Hall mobility, electrical resistivity along with grain size, optical band gap and elemental ratio of CdS thin films as a function of growth temperature is presented in Table 3. Hall effect studies showed that there is a diminutive variation of carrier concentration 5.12 × 10^{14} cm^{-3} to 1.58 × 10^{14} cm^{-3} as the substrate temperature increases from 25 °C to

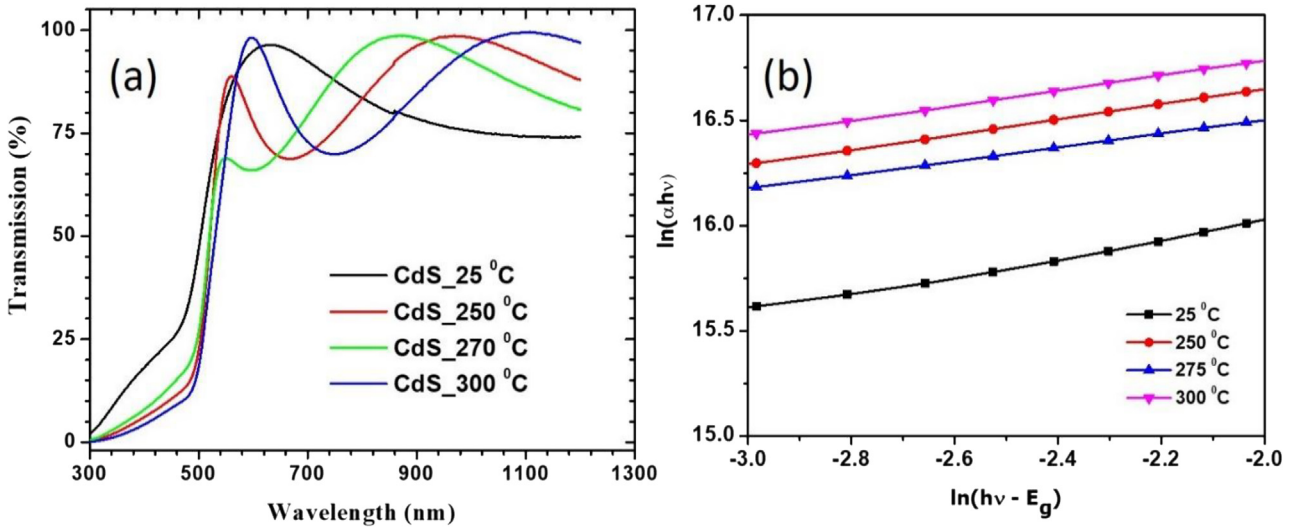

Fig. 4. (a) Optical transmittance spectra of CdS thin films grown at different substrate temperatures (b) Plot of ln(αhν) versus ln(hν- Eg).

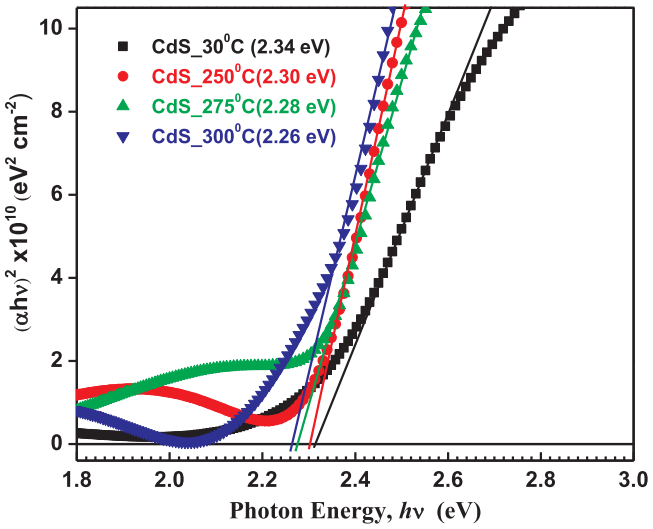

Fig. 5. Optical band gap of CdS thin films grown at different substrate temperatures.

300 °C due to decrement of Cd interstitial defect densities. The decremented trend of Cd vacancies were confirmed from EDX spectra as presented in Fig. 3. The reduction of carrier concentration with substrate temperature is consistent with previous report [15]. In addition, carrier mobility of CdS thin film increased with substrate temperature due to the improved crystallinity and the grain size of the films as depicted in Fig. 6.

From Table 4, it is seen that the resistivity is decreasing with increasing substrate temperature due to the increment of crystallite size and grain size of the deposited CdS thin films. It is well known that the resistivity of the polycrystalline material directly related to the grain boundaries rather than their orientation. The resistivity (ρ) of the polycrystalline CdS thin films can be defined by considering the scattering of electron by the grain boundaries and scattering at the surface. According to Matthiessen's rule the conduction of electron in a polycrystalline material can be defined [44] by:

$$\frac{1}{l} = \frac{1}{l_{crystal}} + \frac{1}{l_{grains}} \tag{9}$$

where l is the average mean free path of electron in the polycrystalline thin films, $l_{crystal}$ is the mean free path of the conduction electron in the single crystal and l_{grains} is approximately equal to average grain size since in a grainy solid, the electron is scattered from grain boundary to grain boundary.

Hence, the resistivity of polycrystalline thin films is inversely proportional to the mean free path which means the resistivity of single crystal ($\rho_{crystal} \propto 1/l_{crystal}$) and resistivity of the polycrystalline sample ($\rho \propto 1/l$). Thus, the resistivity of CdS thin films can be defined as follows:

$$\rho = \rho_{crystal}\left(1 + \frac{l_{crystal}}{l_{grain}}\right) \tag{10}$$

Eq. (10) implies that the resistivity of the polycrystalline sample decreases with the increase of grains size. In our case, we found that the crystallinity of the films improved whereas micro-strain and dislocation densities decrease at elevated temperature which in turn increases the crystallite size and grain size. As the grain size increased with higher temperature, recrystallization occurred during films growth and the minor grains are disappeared. As the grain boundaries reduced at elevated temperature, the resistivity of CdS thin films decreased sharply with the increment of grain size. The correlation between the grain size and the resistivity of the CdS thin film is presented in Fig. 7. The reported result agrees with the other reported works [31,45–47].

Conclusion

In this study, CdS films were deposited by RF magnetron sputtering for substrate temperatures from 25 °C to 300 °C. The structural studies revealed the polycrystalline nature for all the deposited films with preferential stable hexagonal wurtzite crystal orientation (0 0 2) plane irrespective of substrate temperature. The crystallite size of as-grown CdS thin films increased with substrate temperature. Moreover, the micro-strain developed due to the atomic dislocations in the unit cell and domain boundaries were decreased with substrate temperature which signifies the improvement of crystallinity. The FE-SEM images of all deposited CdS thin films indicate the uniform coverage, very compact and pinhole free adhesion to the glass substrate. The compositional studies of the as-grown CdS thin films revealed the Cd-rich stoichiometry. All the deposited CdS thin films showed a sharp transition in optical transmission at the band edge of 520 nm and exhibit transmission over 75%, which signifies the maximum amount of sunlight admitting into the active region of thin film solar cells. In addition, the band gap of the CdS thin films narrowed down from 2.34 eV to 2.26 eV with substrate temperature from 25 °C to 300 °C. Furthermore, all the deposited films demonstrated n-type conductivity. The carrier concentration of as-grown CdS thin film decreased slightly from 5.12×10^{14} cm^{-3} to 1.58×10^{14} cm^{-3} with the increase of substrate temperature. The resistivity of deposited films decreased sharply from 2.77 kΩ·cm to 0.93 kΩ·cm with the increment of substrate temperatures. Additionally, the electron mobility of the as-grown films increased with the growth temperature. Both mobility and resistivity improved with substrate temperature which might be due to the enlargement of crystallite size and reduction in grain boundaries in the deposited films at elevated temperature. Considering the structural, optical and electrical properties, it can be concluded that the films deposited at 300 °C possess higher potentiality to be utilized as a suitable window layer for thin film solar cell application.

Authors contributions

N. K. Das, J. Chakrabartty, and S. Farhad contributed to the experiments, analysed the experimental data and wrote the manuscript. A. K. Sen Gupta helped in thin film deposition process. E. Ahamed contributed to obtain the SEM images. K. S. Rahman, A. Wafi, and A. A. Alkahtani contributed to XRD and UV-VIS experiments. All authors read and comment on the manuscript. J. Chakrabartty led the work towards publication.

Table 3
Crystallite size, Grain size, band gap, and elemental composition of CdS thin films grown at different substrate temperatures.

Substrate temperature (°C)	Crystallite size D (nm)	Avg. grain Size (nm)	Band gap (eV)	Cd (at %)	S (at %)	Cd/S ratio
25	22.87	64	2.34	53.37	46.63	1.14
250	23.49	80	2.30	52.36	47.64	1.10
275	24.16	84	2.28	52.17	47.83	1.09
300	24.58	135	2.26	51.88	48.12	1.08

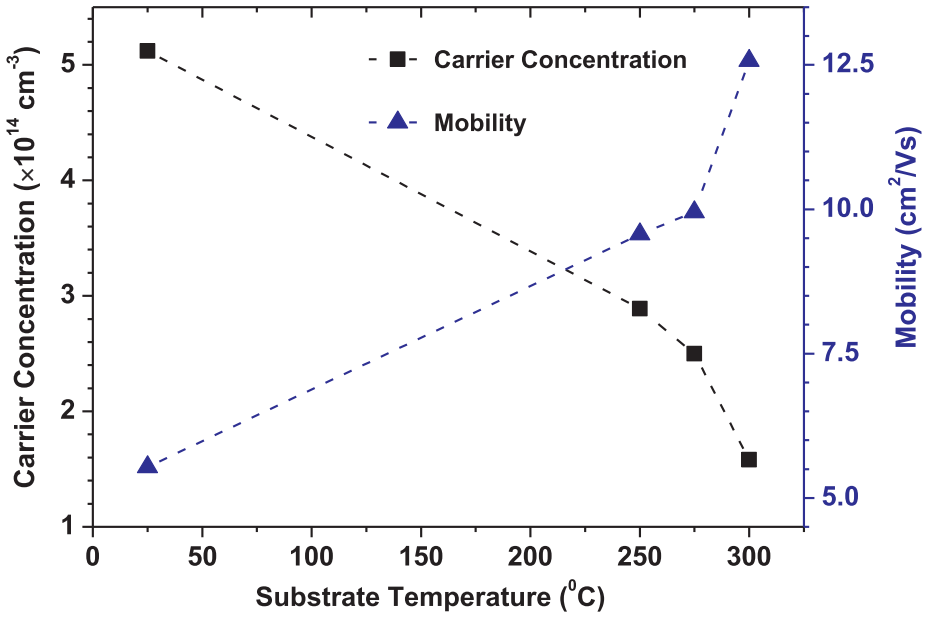

Fig. 6. Effect of substrate temperature on carrier concentration and carrier mobility.

Table 4
Grain size, optical band gap, carrier concentration, Hall mobility, resistivity and elemental ratio of CdS thin films as a function of growth temperature.

Substrate temperature (°C)	Band gap E_g (eV)	Carrier concentration ($\times 10^{14}$ cm^{-3})	Hall mobility ($cm^2/V{\cdot}s$)	Cd/S ratio	Resistivity(kΩ.cm)	Avg. grain size (nm)
25	2.34	5.12	5.53	1.14	2.77	64
250	2.30	2.89	9.57	1.10	2.74	80
275	2.28	2.50	9.95	1.09	2.50	84
300	2.26	1.58	12.57	1.08	0.93	135

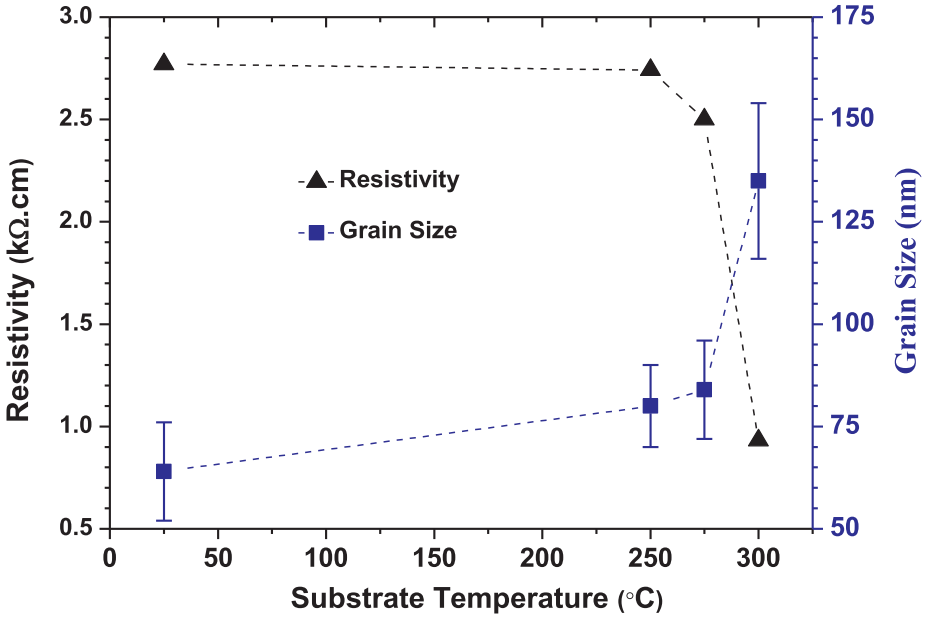

Fig. 7. Variation of electrical resistivity and grain size of the CdS thin films grown at different substrate temperatures.

Declaration of Competing Interest

The authors declare that they have no known competing financial interests or personal relationships that could have appeared to influence the work reported in this paper.

Acknowledgements

The authors acknowledge the Department of Electrical and Electronic Engineering of Chittagong University of Engineering and Technology (CUET) for the thin film deposition facilities. The authors also express sincere thanks to Energy Conversion and Storage Research (ECSR) section of Industrial physics division, Bangladesh Council of

Scientific and Industrial Research (BCSIR) for their support in characterizing the samples. Appreciations are also credited to the Institute of Sustainable Energy (ISE) of the Universiti Tenaga Nasional (@The Energy University), Malaysia for providing characterization supports for this work.

References

[1] Bosio A, Rosa G, Romeo N. Past, present and future of the thin film CdTe/CdS solar cells. Sol Energy 2018;175:31–43.
[2] Akcay N, Zaretskaya E, Ozcelik S. Development of a CZTS solar cell with CdS buffer layer deposited by RF magnetron sputtering. J Alloys Compd 2019;772:782–92.
[3] Guo Y, Jiang J, Zuo S, Shi F, Tao J, Hu Z, et al. RF sputtered CdS films as independent or buffered electron transport layer for efficient planar perovskite solar cell. Sol Energy Mater Sol Cells 2018;178:186–92.
[4] Arepalli V, Kim J. Effect of substrate temperature on the structural and optical properties of radio frequency sputtered tin sulfide thin films for solar cell application. Thin Solid Films 2018;666:34–9.
[5] Sivaraman T, Narasimman V, Nagarethinam V, Balu A. Effect of chlorine doping on the structural, morphological, optical and electrical properties of spray deposited CdS thin films. Prog Nat Sci Mater Int 2015;25:392–8.
[6] Mahabaduge H, Wolden C. Properties of reactively sputtered oxygenated cadmium sulfide (CdS:O) and their impact on CdTe solar cell performance. J Vac Sci Technol A Vacuum Surf Film 2014;33:021203.
[7] Abbas A, Meysing D, Reese M, Barnes T, Walls J, Wolden C. Structural and chemical evolution of the CdS: o window layer during individual CdTe solar cell processing steps. Sol Energy 2018;159:940–6.
[8] Ferekides C, Balasubramanian U, Mamazza R, Viswanathan V, Zhao H, Morel D. CdTe thin film solar cells: device and technology issues. Sol Energy 2004;77:823–30.
[9] Wu X. High-efficiency polycrystalline CdTe thin-film solar cells. Sol Energy 2004;77:803–14.
[10] Paudel N, Yan Y. Enhancing the photo-currents of CdTe thin-film solar cells in both short and long wavelength regions. Appl Phys Lett 2014;10511:183510–92851.
[11] J. Kephart, R. Geisthardt, and W. Sampath, "Sputtered, Oxygenated CdS Window Layers for Higher Current in CdS/CdTe Thin Film Solar Cells," 38th IEEE Photovoltaic Specialists Conference, pp. 854–858, 2012.
[12] Han J, Spanheimer C, Haindl G, Fu G, Krishnakumar V, Schaffner J, et al. Optimized chemical bath deposited CdS layers for the improvement of CdTe solar cells. Sol Energy Mater Sol Cells 2010;95:816–20.
[13] Paudel N, Grice C, Xiao C, Yan Y. The effects of high temperature processing on the structural and optical properties of oxygenated CdS window layers in CdTe solar cells. J Appl Phys 2014;116:044506.
[14] Paudel N, Xiao C, Yan Y. Close-space sublimation grown CdS window layers for CdS/CdTe thin-film solar cells. J Mater Sci Mater Electron 2014;25:1991–8.
[15] Das N, Farhad S, Chakaraborty J, Gupta A, Dey M, Al- Mamun M, et al. Structural and optical properties of RF-sputtered CdTe thin films grown on CdS:O/CdS bilayers. Int J Renew Energy Res 2020;10:293–302.
[16] Salim H, Olusola O, Dharmadasa I, Madugu M, Ojo A. Effect of thickness: a case study of electrodeposited CdS in CdS/CdTe based photovoltaic devices. J Mater Sci Mater Electron 2016;28:3254–63.
[17] Isik M, Gullu H, Delice S, Parlak M, Gasanly N. Structural and temperature-dependent optical properties of thermally evaporated CdS thin films. Mater Sci Semicond Process 2019;93:148–52.
[18] S. Kalogirou, CdTe Solar Cells, McEVOY'S Handbook of Photovoltaic's Fundamentals and Applications, 3rd ed. London, Academic Press, Ch. I-3-B, pp. 309-400, 2018.
[19] Paudel N, Yan Y. Fabrication and characterization of high-efficiency CdTe-based thin-film solar cells on commercial SnO_2:F-coated soda-lime glass substrates. Thin Solid Films 2013;549:30–5.
[20] Genişel M, Bozkaplan C, Akkilic K, Tombak A, Ocak Y. The influence of substrate temperature on RF sputtered CdS thin films and CdS/p-Si heterojunctions. Mater Sci Semicond Process 2016;58:34–8.
[21] Kim D, Park Y, Kim M, Choi Y, Park YS, Lee J. Optical and structural properties of sputtered CdS films for thin film solar cell applications. Mater Res Bull 2015;69:78–83.
[22] Rondiya S, Rokade A, Funde A, Kartha M, Pathan H, Jadkar S. Synthesis of CdS thin films at room temperature by RF-magnetron sputtering and study of its structural, electrical, optical and morphology properties. Thin Solid Films 2017;631:41–9.
[23] Li Y, Ji P, Song Y, Zhou F, Yuan S, Wen N, et al. Fabrication and electrical properties of (002)-oriented grown CdS/Si heterojunctions by radio frequency magnetron sputtering. Mater Lett 2018;228:463–5.
[24] Mis-Fernández R, Peña J, Loeza-Poot M, Camacho-Espinosa E, Rimmaudo I. Enhanced uniformity of sputtered oxygenated cadmium sulfide (CdS:O) films for large area photovoltaic applications. Sol Energy 2018;173:1025–31.
[25] Xiao J, Wen B, Melnik R, Kawazoe Y, Zhang X. Phase transformation of cadmium sulfide under high temperature and high pressure conditions. Phys Chem Chem Phys 2014;16:14899–904.
[26] Williamson G, Smallman R. III. Dislocation densities in some annealed and cold-worked metals from measurements on the X-ray Debye-Scherrer spectrum. Philos Mag 1956;1:34–46.
[27] Alfonso E, Olaya J, Cubillos G. Thin film growth through sputtering technique and its applications. Book Chapter of Crystallization Science and Technol.. IntechOpen; 2012.
[28] Khatter J, Chauhan R. Effect of temperature on properties of cadmium sulfide nanostructures synthesized by solvothermal method. J Mater Sci Mater Electron 2020;31:2676–85.
[29] Makhdoumi-Kakhaki Z, Youzbashi A, Sangpour P, Naderi N, Kazemzadeh A. Effects of film thickness and stoichiometric on the electrical, optical and photodetector properties of CdS quantum dots thin films deposited by chemically bath deposition method at different bath temperature. J Mater Sci Mater Electron 2016;27:12931–9.
[30] Rondiya S, Rokade B, Gabhale S, Pandharkar M, Chaudhari A, Date M, et al. Effect of bath temperature on optical and morphology properties of CdS thin films grown by chemical bath deposition. Energy Procedia 2017;110:202–9.
[31] Shah N, Ray J, Desai M, Panchal C. Influence of substrate temperature on structural, optical and electrical properties of evaporated cadmium sulphide thin films. J. Optptoelectronic. Adv. Mat. 2010;12:2052–6.
[32] Tsai C, Chuu D, Chen G, Yang S. Studies of grain size effects in rf sputtered CdS thin films. J Appl Phys 1996;79:9105–9.
[33] Islam M, Hossain M, Aliyu M, Chelvanathan P, Huda Q. Comparison of structural and optical properties of CdS thin films grown by CSVT, CBD and sputtering techniques. Energy Procedia 2013;33:203–13.
[34] Hussain T, Al-Kuhaili M, Durrani S, Qayyum H. Effect of collision during vapor transport between Cd and X (X = Te2, Se2, or S2) molecules on the properties of thermally evaporated CdTe, CdSe, and CdS thin films. Results Phys 2018;8:988–1000.
[35] D. Hemenway, "Computational modeling of cadmium sulfide deposition in the CdS/CdTe solar cell manufacturing process," Dept. Mech. Eng., Colorado State Univ. Colorado, 2013.
[36] Ouachtari F, Rmili A, Elidrissi B, Bouaoud A, Erguig H, Elies P. Influence of bath temperature, deposition time and S/Cd ratio on the structure, surface morphology, chemical composition and optical properties of CdS thin films elaborated by chemical bath deposition. J Mod Phys 2011;02:1073–82.
[37] Toma O, Ion L, Iftimie S, Radu A, Antohe S. Structural, morphological and optical properties of rf – Sputtered CdS thin films. Mater Des 2016;100:198–203.
[38] Chowdhury R, Hossen M, Mustafa G, Hussain S, Rahman S, Farhad S, et al. Characterization of chemically deposited cadmium sulfide thin films. Int J Mod Phys B 2010;24:5901–11.
[39] Manifacier J, Murcia M, Fillard J, Vicario E. Optical and electrical properties of SnO_2 thin films in relation to their stoichiometric deviation and their crystalline structure. Thin Solid Films 1977;41:127–35.
[40] Coulter J, Birnie D. Assessing tauc plot slope quantification: ZnO thin films as a model system. Phys Status Solidi Basic Res 2018;255:1–7.
[41] Ikhmayies S, Ahmad-Bitar R. A study of the optical band gap energy and Urbach tail of spray-deposited CdS: In thin films. J Mater Res Technol 2013;2:221–7.
[42] Suryavanshi P, Panchal C. Investigation of urbach energy of CdS thin films as buffer layer for CIGS thin film solar cell. J Nano- Electron Phys 2018;10:02012–2017.
[43] Werta S, Echendu O, Dejene F, Urgessa Z, Botha J. Temperature-dependent properties of electrochemically grown CdS thin films from acetate precursor. Appl Phys A Mater Sci Process 2018;124.
[44] Kasap Safa, Capper Peter, editors. Springer Handbook of Electronic and Photonic Materials. Cham: Springer International Publishing; 2017.
[45] Jassim S, Zumaila A, Waly G. Influence of substrate temperature on the structural, optical and electrical properties of CdS thin films deposited by thermal evaporation. Results Phys 2013;3:173–8.
[46] Kathirvela D, Suriyanarayanan N, Prabahar S, Srikanth S. Structural, electrical and optical properties of CdS thin films by vacuum evaporation deposition. J Ovonic Res 2011;7:83–92.
[47] Zahra S. Effect of grain size on the electrical conduction mechanism for aluminum doped CdS thin films. J Electron Devices 2013;17:1494–9.